Published in final edited form as:
Langmuir. 2012 March 6; 28(9): 4373–4381. doi:10.1021/la205084z.

Silk-silica composites from genetically engineered chimeric proteins: materials properties correlate with silica condensation rate and colloidal stability of the proteins in aqueous solution

David J. Belton[1], **Aneta J. Mieszawska**[2], **Heather A. Currie**[1,2], **David L. Kaplan**[2], and **Carole C. Perry**[1,*]

[1]Biomolecular and Materials Interface Research Group, Interdisciplinary Biomedical Research Centre, School of Science and Technology, Nottingham Trent University, Clifton Lane, Nottingham UK NG11 8NS

[2]Department of Biomedical Engineering, Bioengineering and Biotechnology Center, Tufts University, 4 Colby Street, Medford, Massachusetts 02155, USA

Abstract

The aim of the study was to determine the extent and mechanism of influence on silica condensation that is presented by a range of known silicifying recombinant chimeras (R5- SSKKSGSYSGSKGSKRRIL; A1- SGSKGSKRRIL; and Si4-1- MSPHPHPRHHHT and repeats thereof) attached at the N-terminus end of a 15 mer repeat of the 32 amino acid consensus sequence of the major ampullate dragline Spindroin 1 (Masp1) *Nephila clavipes* spider silk sequence ([SGRGGLGGQG AGAAAAAGGA GQGGYGGLGSQG]$_{15}$X). The influence of the silk/chimera ratio was explored through the adjustment of the type and number of silicifying domains, (denoted X above), and the results were compared with their non chimeric counterparts and the silk from *Bombyx mori*. The effect of pH (3–9) on reactivity was also explored. Optimum conditions for rate and control of silica deposition were determined and the solution properties of the silks were explored to determine their mode(s) of action.

For the silica-silk-chimera materials formed there is a relationship between the solution properties of the chimeric proteins (ability to carry charge), the pH of reaction and the solid state materials that are generated. The region of colloidal instability correlates with the pH range observed for morphological control and coincides with the pH range for the highest silica condensation rates. With this information it should be possible to predict how chimeric or chemically modified proteins will affect structure and morphology of materials produced under controlled conditions and extend the range of composite materials for a wide spectrum of uses in the biomedical and technology fields.

Introduction

The use of alien materials in the human body has increased dramatically over the past 50 years although the origin of their use dates at least to the time of the pharaohs who used

*Corresponding author: C.C. Perry, Biomolecular and Materials Interface Research Group, Interdisciplinary Biomedical Research Centre, School of Science and Technology, Nottingham Trent University, Clifton Lane, Nottingham UK NG11 8NS, Phone: 00 + 44 115 8486695, Fax: 00 + 44 115 8486616, Carole.Perry@ntu.ac.uk.

Supporting information
Buffer comparison for scattering data, changes in silicic acid concentration with time, silicic acid, protein concentrations at equilibrium and analytical details, SEM of silica formed from buffered TEOS alone, FTIR of 15 mers and an example and statistics of amide I band fitting as well as a table of data on the pH at which isolable material was recovered from silicifying systems is provided free of charge via the Internet at http://pubs.acs.org

natural silk for sutures and more recently 150 years ago when amalgam dental fillings were first used.[1] Over the years these materials have become more sophisticated with biocompatibility and bio-acceptance being important. Silks provide a valuable natural source of biomaterials that can be fabricated into differing physical forms including fibres, films and gels for physiological applications for controlled release[2–4] and as tissue engineering constructs.[5–9] In addition to being well tolerated biologically[10–12] silk has many physical properties which are highly valued such as its elasticity and tensile strength.[13–15] In the last 20 years there has been growing interest in understanding the properties of silks with a view to generating new materials based on spider silks and bioengineered variants of silkworm and spider silks.[16] Although spiders produce a wide range of silks[17] having different functions such as protection for the lining the egg case (aciniform silk); some are more glue like (pyriform and aggregate silks) while others have a more structural role such as the major and minor ampullate silks used in the web and draglines, none have been commercialised due to the difficulty of domestication of the cannibalistic Araneae. Silks have impressive mechanical properties of strength and toughness that rivals those of synthetic high performance fibers such as Kevlar,[18] however in compression none of the silks perform well as fibres or in highly porous gel networks as under these conditions they are less resistant to compressive deformation.

Amorphous silica is an inorganic material which is well accepted biologically[19] and is found in nature as various silicate minerals and in its soluble form, $SiOH_4$ (orthosilicic acid, also sometimes called monosilicic acid) in all water sources at concentrations ranging from a few parts per million (ppm) up to approximately 100 ppm. It is from this source that many organisms are able to sequester silica to form structural materials. Diatoms for example form elaborate shells (thecae) which provide structure and protection whilst still allowing the diffusion of nutrients and gases. The controlled deposition of silica in organisms such as diatoms involves a number of proteins and shorter peptides that include post translationally modified silaffins.[20] These have been shown to promote silica formation *in vitro*. As an example, Silaffin 1A (a 19 amino acid peptide containing polyamine modified lysine groups) has been shown to regulate silica deposition and morphology from pre hydrolysed tetraalkoxysilane solutions *in vitro*,[21] a property also shared with its synthetic non modified counterpart, R5, (SSKKSGSYSGSKGSKRRIL).[22] In addition the same study found that fragments of the R5 peptide such as the 11 mer, SGSKGSKRRIL (A1) had similar effects. Other unrelated peptides with silicifying ability have also been identified by screening methods (phage display) to isolate peptide sequences which show binding affinity to silica surfaces. One example, MSPHPHPRHHHT (Si4-1 or A3),[23] showed the greatest activity in terms of the level of silica deposition from pre-prepared orthosilicic acid solutions when compared with a number of other silica binding phage peptide sequences.

Silica is itself a brittle material with poor tensile properties but it is hard and can be used in composite materials to complement the inherent properties of other components. The possibility of forming silk scaffolds with controllable porosities using silica to impart structural rigidity could potentially provide biomedical science with a range of slowly bio-degradable implantable materials that also have the capacity for doping with growth factors, nutrients or targeted drugs to be released during the lifetime of the implant.[24]

In principle, silk-silica composites could be tailored using the bio-inspired silicification process performed *in vitro* at circum-neutral pH and ambient temperature. In our earlier studies using the 32 amino acid consensus sequence of the major ampullate dragline Spindroin 1 (Masp1) *Nephila clavipes* spider silk sequence ([SGRGGLGGQG AGAAAAAGGA GQGGYGGLGSQG]$_n$) and a silica binding peptide (R5-SSKKSGSYSGSKGSKRRIL)) we have shown that protein chimeras can be generated using genetic engineering and further demonstrated the positive effect of the binding peptide on

the silicifying properties of silk.[25] We have more recently shown that these materials promote osteoblast development with the up regulation of key markers associated with bone formation.[26]

To further advance the potential application of such spider silk-silica composite materials for applications including those in biomedical science knowledge of the reaction environment available for silica formation is needed together with an understanding of the compatibility of silica formation with maintenance of the excellent structural characteristics of the silk itself such as its microcrystalline β sheet structure which confers some of its impressive mechanical properties. In this contribution we therefore consider the effect of the identity of the peptide used on silica formation and on the structure of the silk component itself. The activity of peptides, (R5- SSKKSGSYSGSKGSKRRIL), a truncated form (A1-SGSKGSKRRIL) and a peptide identified by Phage display (Si4-1 or A3-MSPHPHPRHHHT), as well as multiples of this sequence as A3(2) and A3(3), were compared to controls; a silk 15-mer without a specific silicifying domain and a native silk fibroin from *Bombyx mori*. The effect of pH (3–9) on composite formation (particle size and size distribution) and protein secondary structure for the silk proteins associated with the siliceous materials are compared. Optimum conditions for rate and controlled silica morphology deposition were determined and the solution properties of the silks were explored to determine their mode(s) of action.

The data show that knowledge of the solution behaviour of the chimeras together with an understanding of silica formation can be used to predict the likely compatibility of the two phases.

Materials and methods

Recombinant silk and chimeras

The 15-mer repeat of the consensus sequence (major ampullate spidroin - MaSp I) from the spider dragline silk (*Nephila clavipes*) (SGRGGLGGQGAGAAAAAGGA-GQGGYGGLGSQGT)$_{(15)}$X where C-terminal domains, X, of A1 (SGSKGSKRRIL-15mer A1), A3(1),(2),(3) (MSPHPHPRHHHT$_{(1-3)}$-15 mer A3(1-3)), R5 (SSKKSGSYSGSKGSKRRIL-15 mer R5) or absent for the non chimera-(15 mer) were prepared using cloning strategies previously described.[25,27] All of the constructs were His tagged for the purpose of purification.

Bombyx mori silk fibroin preparation

The silk materials were prepared using our previously reported procedures.[28] Briefly, silk cocoons were degummed using 0.5% sodium carbonate solutions and water washing and the separated silk fibres dried in air. The silk fibroin was regenerated by dissolving in lithium bromide solution (9M) to ~5% protein concentration, dialysing rapidly (<8 hours) against distilled deionised water to a conductivity of <10 μS/cm and finally freeze drying.

Turbidity measurements

To compare the effects of the silk and chimeras on the condensation and precipitation of silica the rate of change in the turbidity (as scattering at 595 nm) during the condensation process was monitored using a Labtech LT-5000 plate reader with Manta software (build 0460). Sarstedt 96 well tissue culture plates were used to allow simultaneous, rapid analysis of small scale reactions with various additives over a range of pH's as well as analysis of control samples under identical conditions.

In a typical reaction, 200 μl of a 1.0 mg/cm^3 silk/chimera solution buffered to pH 3–9 with 0.1 M tris bis propane/citric acid buffers was pipetted into the required wells and then 6 μl of pre-hydrolysed tetraethoxy silane (TEOS) solution added (2.23 cm^3 TEOS dispersed in and diluted to 9.9 cm^3 with 50% aqueous ethanol, 100 μl 1 M HCl added and allowed to hydrolyse for 10 minutes) to give a final [$Si(OH)_4$] of 30 mM. Scattering, measured as the absorbance at 595 nm, was continuously monitored over 48 hours. Control samples in addition to the 15 mer and regenerated bombyx fibroin included buffered condensing silica solutions over the same pH range. Measurements were also made on solutions buffered with phosphate at identical concentrations and pH. Although typically a phosphate buffer is employed by others[20,21] for these types of studies, a bis tris propane/citrate buffer system was preferred as it enabled the monitoring of pH effects over the complete pH range 3–9 and did not lead to complications in mixed buffer recipes. Furthermore the two systems (bis tris propane/citrate and phosphate) did not show significant differences in the scattering profiles when compared, Figure 1 supplemental.

The condensed silica/chimeras from each well were isolated at equilibrium (determined by the molybdenum blue colorimetric method - details in supporting information) by centrifugation (5 minutes at 13,000 rpm) and washed twice with water followed by further centrifugation and finally freeze dried.

Scanning electron microscopy

The morphology and size of the particles was assessed using scanning electron microscopy. Small amounts of sample were dusted on to electrically conducting carbon sticky patches mounted on aluminium stubs and then gold coated using an argon gold plasma at 1.2 kV for 2 minutes (estimated to provide a gold coating of 5–10 nm). Images were collected using a Jeol 840 scanning electron microscope with a tungsten filament and a beam acceleration voltage of 20 kV coupled with an Oxford Instruments Inca x-ray microanalysis suite for elemental analysis. Particle size analysis was carried out by averaging the diameter of 50+ particles and calculating the diameter standard deviation.

FTIR-ATR (Fourier Transform Infrared Attenuated Total Reflectance Spectroscopy) analysis

FTIR-ATR was used to assess the effect of pH on protein conformation, to identify the presence of silica in the samples and to assess the effect of composite formation on protein conformation. For the study of pH on protein conformation, samples were dissolved in 0.3 M potassium chloride solutions which contained pre-added amounts of HCl or KOH to obtain the required final pH of solution (volumes pre-determined by titrimetry). The solutions were then allowed to stand for 30 minutes before flash freezing with liquid nitrogen and then freeze drying. This method for pH control was preferred to the use of buffers such as bis tris propane/citrate which introduce additional bands in the spectrum in the carbonyl region and make isolation of the spectral contributions from the amide bands impossible to obtain. This process unfortunately makes circumneutral pH difficult to achieve so no data was available between pH 5.5 and 7.8 for the chimeric silks. FTIR-ATR used a single reflection diamond ATR assembly, data were collected at a resolution of 4 cm^{-1} and 16 scans were averaged (4000–380 cm^{-1}). Silica/silk composites were isolated by centrifugation (5 minutes at 3000 rpm) and 2 × water washes to remove extraneous silk and buffer and then freeze dried. Infrared spectra were then collected as detailed above.

Curve fitting was performed using Thermo Grams A1 software v8.0. Spectral baselines were corrected (levelled and zeroed) and spectra smoothed where necessary (binomial 10–15 points). Six points were selected across the amide 1 band (1700–1580 cm^{-1}), 4 for each of the conformer absorbances (β turn 1690–1662 cm^{-1}, α helix 1662–1645 cm^{-1}, random coil

1645–1637 cm^{-1} and β sheet 1637–1613 cm^{-1}).[29–34] The two additional absorbances were allocated for side chain compensation (1710–1690 cm^{-1}) and non baseline separation of the amide I and amide II bands (1610–1590 cm^{-1}). The absorbance bands were confined within these limits and further width limited to between 8 and 30 cm^{-1} at half height. After loading the parameters a single iteration was carried out to force all peaks to have a positive area value and a linear baseline selected. A further 1000 iterations were then carried out to fit the curve. The areas under the identified conformer peaks were summed and each conformer expressed as a percentage of the total. The reproducibility of the sampling procedure, data handling and peak fitting analysis was tested using three commonly used proteins having different proportions of the main secondary structure types (γ globulin, α lactalbumin and bovine serum albumin). 5 replicate analyses were carried out on each protein type and error bars constructed to represent 95% confidence interval (2σ) for each conformation quantified. The errors associated with this type of analysis are illustrated in Figure S6 supplemental for α lactalbumin.

Zeta potential measurements

Zeta potential measurements were used to measure the charge of the proteins over the pH range 3–9. Solutions of the chimeric proteins were made in aqueous 0.1 M citric acid solutions to a concentration of 1 mg/cm^3 and then filtered through a 450 nm membrane to remove any undispersed aggregates. Measurements were made using a Malvern nanoS Zetasizer, a dispersed phase properties of latex and a dispersion phase of 0.1 M tris buffer were chosen for a compatible refractive index, viscosity and dielectric constant. Five separate measurements were made at each pH and the results averaged (any outliers were removed where necessary but not more than one allowed per data set). The pH was adjusted for subsequent measurement by the addition of measured amounts of 1.0 M tris bis propane and the measurements repeated to give zeta potential data over a pH range 3–9. The *B. mori* fractions tended to gel rapidly in the citric acid solution so they were first prepared in 0.1 M tris bis propane buffer and the pH adjusted down after each measurement by the addition of measured amounts of 1.0 M citric acid solution. Otherwise the conditions used were the same as for the chimeras.

Results and discussion

Sequence variations from nature and from phage display results for silica[23] suggest that the chemical identity of the domain involved in silica formation will affect the nature of the silica morphology generated. In prior studies silica formation under physiological conditions (pH *ca*. 7) have been reported.[25,26] In the present study the full pH range over which silica formation occurs is identified, as well as the time dependent course of the reactions. The formation of silica from orthosilicic acid is described by Iler.[36] Essentially this is a process driven by the formation of anionic silicate species the pK_a of which decreases with the level of condensation and results in the formation of primary particles, the fate of which depends further upon pH and ionic strength. For a silicified material to form rapidly the reaction is normally carried out under neutral to mildly basic conditions, but if condensation is observed under a wider pH regime this can suggest that the pathway for condensation is being modified by other species present in solution. In this case, we will see that the solution properties of the silk and silk-based chimeric proteins under equivalent reaction conditions are important. As the chimeras contain basic amino acids (plus acidic amino acids for silk fibroin), Table 1, their properties including their ability to carry charge are affected by pH, ionic strength and the protein primary structure. Further, their interplay determines the secondary structure adopted by the protein which in turn may affect how these molecules are able to interact with silica particles as they develop.

Due to the very small scale reactions that were performed simultaneously to compare the activity of the chimeras over a range of pH values, scattering intensity at 595 nm was taken as a measure of the extent of and rate of reaction with data being shown in Figure 1. Scattering is a function of the number and size of particles in suspension, with a ten-fold increase in particle diameter resulting in a 10^6 increase in intensity [described by Rayleigh scattering for particles much smaller than the wavelength of light or Mie theory for larger particles]. The silk solutions scatter light due to the size of the silk molecules (silk fibroin ~ 10nm, genetic chimeras ca. 2–3 nm) but unless aggregation occurs the apparent absorbance due to scattering at the wavelength of observation (595 nm) is minimal. It is only when particles begin to grow or aggregate that the scattering becomes significant. Similarly, for the condensing silica system used in this study (30mM buffered TEOS) 2–4 nm particles are produced which only begin to significantly affect the measured absorbance as they start to aggregate after an hour or more of reaction. Scattering observed at shorter times than one hour indicates an interaction of the silk or silk based chimeras with the silicifying system. This interaction may be in the form of aggregation control or a modification of the condensation process. At fixed ionic strength, additives which exhibit aggregative effects rarely show any control of the primary particle size which remain in the region of a few nm in diameter although their assembly may be affected.

Even after only 5 minutes of reaction, Figure 1a and c, the level of scattering observed from samples containing the chimeric silks indicates the formation of particles or aggregates of considerable size at pH *ca*. 6–8 where silica condensation is known to be fastest.[36] At slightly more acidic conditions (pH *ca*. 6), a more modest increase in absorbance was noted for the 15 mer alone (with His tag) but not for condensation performed in the presence of regenerated fibroin. To have large (100's nm diameter) particles form in this short time under these reaction conditions is very unusual. Associated with the large increase in absorbance at 595 nm was a much more rapid reduction in the levels of orthosilicic acid than was observed for samples where such large increases in absorbance were not observed, Figure 2 supplemental suggesting that the scattering was not due merely to increased aggregation rates but possibly to some catalytic activity exerted by the chimeras on the silica condensation process. The chemical identity of the silicifying component of the chimera had an effect on the absorbance under very mildy acidic conditions (pH 6.5) in a manner that could be largely equated with the number of basic amino acids present, Table 1, with 15mer-R5 and 15mer-A3 being more active than 15mer-A1 and 15-mer silk. Additionally, the presence of multiple A3 groupings in the 15-mer silk constructs –15 mer A3(2) and -15 mer A3(3) also increased the absorbance measured for silicifying systems at circumneutral (6.5 – 7.5) pH. By equilibrium, Figure 1b and d, the pH range over which large particle/aggregate formation was observed had extended to between pH 4 and 9 but the differences in behaviour observed between the contrasting chimeras had largely disappeared. The scattering observed for all samples at pH 3.1 suggests the formation of small poorly scattering particles and the absence of residue in most of the samples after centrifugation tends to support this (sub 50 nm particles of silica are not expected to be sedimented at 3000 rpm). Where material was isolable the structure was found to be largely poorly controlled random aggregates making up < 10% of the expected condensable silica. In the absence of additives silica particles of the size required to generate the higher levels of scattering only form under neutral to basic conditions of low ionic strength (<0.1 molal). [37] The effect of a single specific silicifying domain on the absorbance measured was less pronounced than for the early time point in the reaction but absorbance for the multiple A3 groups attached to the silk 15-mer remained at a higher level than for other chimeras. At the highest pH measured (*ca*. 9), a distinct difference in scattering between the 15mer-silica materials and the chimera-silica materials was observed with the chimeric constructs maintaining much of their ability to form aggregates/structures that were of sufficient size to scatter light at 595 nm. The low level scattering (abs ~0.15) observed for the 15mer silk in the absence of added

silicate precursor indicates scattering caused by molecular protein in the pH range 4.5–8. Scattering observed for the silicifying systems in the presence of the regenerated *B. mori* remained low indicating the presence of silk molecular colloids and small primary silica particles rather than any larger silica particles as observed with the chimeric proteins. Confirmation of the structures formed and their composition was obtained by a combination of electron microscopy/EDXa analysis and FTIR studies of the solids combined with analysis of the solution phase for residual protein (Bradford assay – details in the supporting data)/uncondensed silicic acid (molybdenum blue assay). In all cases, reaction between the condensing silica system and the chimeras lead to an almost total removal of orthosilicic acid from the system down to 0.2–0.4 mM, well below the solubility limit, Figure 3 supplemental. Virtually all protein was removed from solution for the rapidly condensing systems between pH 6–8, Figure 4 supplemental.

Silica morphology

The effect of silicifying domain identity and pH on structures formed was followed by scanning electron microscopy. Figure 2 shows examples of the effect of pH on the nature of the structures detected for each of the 15mer proteins and the regenerated *B. mori* fibroin and an example EDXa spectrum of the precipitates confirming the presence of ‘Si’, ‘N’ and ‘C’ is provided. Figure 3 shows the effect of pH and chimera identity on mean particle size, and particle size distribution, Figure 3a shows the effect of different chimeras and Figure 3b the effects of chimera extension. Examples of the effect of pH on the nature of silica formed in the absence of silk/silk chimeras is shown in Figure 5 supplemental. At pH *ca*. 3 aggregation of silica decorated silk structures was observed but with poor control of size and shape and low yield suggesting the majority of the silica condensed was in the form of small particles not isolable by centrifugation. At pH values of *ca*. 4–8, distinct spherical particles were observed for all chimeras that varied in size and size distribution according to the specific silicifying domain attached to the end of the consensus silk sequence. For pH values above this and up to pH 9 larger spherical particles were observed showing more varied levels of control over size dispersity. At higher values still dispersed structures containing few spheres were observed with significantly reduced yields. For the chimeras studied, the smallest particles with the smallest particle size distribution were found for 15 mer A1 (the truncate of R5) over all pH ranges and with minimum particle diameter and size dispersity at pH~7. The largest particles were found for 15 mer R5 and the effect of additional silicifying units (15 mer A3, A3(2), A3(3) had a modest effect on average particle size with a broadening of the particle size distribution observed. In all cases, the most regular particles with minimum particle size and standard deviation (i.e. tightest morphological control) occurred between pH 7 and 8 with particles of between ca. 800 nm and 2 μm and dispersity of ± 10% being produced, according to the identity of the silicifying domain. For the controls, silica precipitated in the absence of the silk proteins but under the same conditions of pH and ionic strength showed only aggregated structures and little observed change with pH. Materials formed in the presence of *B. mori* silk did not vary significantly with pH (isolable residue only recoverable at pH 4.7 to 7.8), Table 1 supplemental, with materials being formed by templating of the protein structure with small silica particles Figure 2. Since both the natural silk and silica particles carry a small negative charge at pH values above 4 there is limited favourable interaction between the two species such that it is likely that the observed materials are formed through entrainment of the silica particles during slow silk aggregation or deposition as a result of the drying process. At the most acidic pH used during condensation (3.1) only the 15 mer A1 and 15 mer R5 single chimeras and the 15 mer A3 multiple silica domains (2), (3) produced any silica residues and these showed poor morphological control.

Protein structure in silk-silica composites

FTIR-ATR was used to explore the effect of pH on the secondary conformations adopted by the chimeras associated with the siliceous deposits, Figure 4. As expected, the precipitates prepared in the presence of the *B. mori* fibroin control showed considerable amounts of beta sheet and beta turn structures compared with the chimeric proteins, Figure 4d. The non chimeric 15 mer showed a small decrease in beta sheet structure on basification but the chimeras showed little effect of pH on the secondary structure of the silk component regardless of the silicifying component(s) present. In all cases, the amount of beta sheet present was reduced compared to the fibroin and the contribution to the spectrum from beta turns was increased. Example spectra are shown in Figure 6 supplemental and a series of plots showing the effect of pH on the proportions of species present provided in Figure 4a–c.

In order to be able to explain and furthermore predict the likely behaviour of specific chimera- mineralising systems we sought to understand the relationships between solution chemistry and the materials formed.

Solution studies- Molecular and particulate charge of the proteins – Zeta potential measurements

The stability of colloidal systems in part depends on the surface charge of the dispersed phase[38–39] in this case the silk proteins, in order to generate sufficient electrostatic repulsive force to prevent onset of the hydrophobic effect and particle aggregation. Particles with zeta potentials of greater than +/−30mV are regarded as increasingly stable whilst those with < +/−5mV potentials are regarded as highly unstable and under these conditions rapid aggregation or coagulation will occur. Natural *B. mori* silk fibroin proteins consist largely of the neutral amino acids glycine, alanine and serine[40–44] (~80% of residues) with the acidic residues of aspartic acid and glutamic acid estimated at ~3% and basic residues arginine, lysine and histidine estimated at ~1%, Table 1. Zeta potential measurements show silk fibroin to have an isoelectric point (pI) just above pH 4 (Figure 5b) and to be negatively charged and increasingly stable as a colloid at higher pH. The range of greatest colloidal instability for silk fibroin is between pH 4 and 5.5 and is demonstrated by rapid gelation of this protein over this pH range.

By comparison, the recombinant chimera silks all show pH shifted isoelectric points ranging from 5.5–8.2. The sequence of increasing pI was fibroin < 15mer < 15mer-R5 < 15mer-A1 ≈ 15mer-A3 < 15mer-A3(2) < 15mer-A3(3). The region of greatest colloidal instability varied according to the chemical identity of the silicifying domain peptide. In the absence of the silicifying domain the range of highest instability is relatively narrow (4.5 – ca. 6.8). For the series of 15 mer A3 chimeras, even though the pI shifts with increase of the number of silicifying domains the range of maximum colloidal instability remains virtually unchanged at ca. pH 5.5 through to pH ca. 9. For the chimera with the R5 peptide attached the region of colloidal instability was further extended from pH 4 through to pH 10. A direct consequence of the ability of the 15mers to resist further charging through the close association of the histidine tags and the basic amino acids (histidine, lysine and arginine) due to localised high charge density in the silicifying domains causes coagulation, coalescence or aggregation of the silk based materials to occur. At the extreme, complete phase separation of the silks could occur but where small residual charge remains there is the possibility for larger aggregated/coalesced structures to become stabilised as the system adjusts to entropic change whilst still compensating for the small charges and it is these small charges that are available to interact with the condensing silica phase. In order to investigate the effect of pH on the secondary structures adopted by the silks in solution, FTIR-ATR studies were

therefore carried out on the various silks treated over a range of pH values to determine if this change in colloidal property was reflected in the protein conformational structure.

Whether the favoured conformation is β sheet, β turn, helical, random coil or, under more extreme conditions of high or low pH, extended chain, these secondary structures in turn determine the solubility of the protein and whether the molecules remain isolated or aggregate to form ordered or disordered structures. In order to produce materials of form and function required it is important to recognise not only the chimeras which modify condensation chemistry and morphology but also to investigate their solution structures at the conditions under which they operate.

Protein conformational study using FTIR-ATR

To assess the effect of the pH on the conformational structures and how this related to the zeta potential measurements the 15mer and 15mer-R5 chimera were compared over a range of pH values, Figure 6.

These were conducted in the absence of the interfering buffer, (KCl was used to match the ionic strength), and without silica precursor in order to monitor the preferred solution conformations of the polypeptides at each of the pH values recorded. Under mildly acidic pH conditions a greater tendency toward β sheet and turn formation was observed which was replaced with random coil/helical structure as the pH increased. In the absence of the terminal silicifying moiety this tendency begins to reverse above pH 4.5 but with R5 present the effect is maintained. It would appear that β sheet and turn structure is preferred when these proteins are stable as colloids but that random coil or helical conformers begin to dominate when they are unstable. However when this data was compared with that of Figure 4 it is clear that the level of beta structure was much reduced in the silica condensate indicating that this ordering is rapidly disrupted by the close association of the protein with the condensing silica matrix.

General discussion and conclusions: Relationship between silk-silica composite particle formation and silk solution behaviour

The rapid formation of large silica particles observed in silicifying systems in the presence of the silk chimeras can be rationalised as the condensation of silica within coagulated protein particles which behave as charge stabilised entropic emulsions. The size of the protein particles produced is a function of residual charge, size of the interfacial surfaces and entropic stress caused by hydrogen bonding disruption and hence each system will have its own intrinsic particle size dependent on the interplay between these factors. The driving force for extensive fast silicification is likely therefore to be the water reduced environment of these protein domains making the removal of water from the silica condensation reactions energetically more favourable. The zeta potential on the *B. mori* fibroin means that it only rapidly aggregates or coagulates at around pH 4 and under these conditions the condensation of silica from orthosilicic acid solution is very slow. At circumneutral pH when the condensation process is more favoured the bombyx fibroin has a zeta potential of <-10mV representing a quasi stable colloidal system showing only slow intermolecular associations and no interaction with the silica condensation process. As a consequence the silica particles formed merely ‘decorate’ the *B. mori* fibroin protein structures on freeze drying.

For the silica-chimeric materials formed there is a relationship between the solution properties of the chimeric proteins, the pH of reaction and the solid state materials that are generated, Figure 7. The region of colloidal instability correlates with the pH range observed for morphological control and coincides with the range of highest silica condensation rates.

With the aid of this information it is possible to begin to predict how chimeric or chemically modified proteins can affect the structure and morphology of materials produced under controlled conditions and extend the range of potential complementary composite components for a wide spectrum of uses. The modification of zeta potential to cause colloidal instability should be possible over a wide range of pH by careful selection of acidic or basic side chains and by using this strategy it will be possible to target a number of different condensing systems and tune the protein instability region to that of maximum condensation rates. Additionally with control of chargeability of the silks by modification of the mineralizing domain it should be possible to optimise the surface charge density and hydrophobic content and in so doing exert morphological control (i.e particle size and dispersity) over the materials formed.

Supplementary Material

Refer to Web version on PubMed Central for supplementary material.

Acknowledgments

Funding from NIH grants R01-DE017207 and EPSRC EP/E048439/1 are gratefully acknowledged.

References

1. Nicholson, JW. The Chemistry of medical and dental materials. Royal Society of Chemistry; Cambridge: 2002.
2. Wenk E, Wandrey AJ, Merkle HP, Meinel L. Silk fibroin spheres as a platform for controlled drug delivery. J Control Release. 2008; 132:26. [PubMed: 18761384]
3. Li W, Mauck RL, Tuan RS. Electrospun nanofibrous scaffolds: production, characterization and applications for tissue engineering and drug delivery. J Biomed Nanotechnol. 2005; 1:259.
4. Okhawilai M, Rangkupan R, Kanokpanont S, Damrongsakkul S. Preparation of Thai silk fibroin/gelatin electrospun fiber mats for controlled release applications. Int J Biol Macromol. 2010; 46:544. [PubMed: 20219530]
5. Gellynck K, Verdonk PCM, Van Nimmen E, Almqvist KF, Gheysens T, Schoukens G, Van Langenhove L, Kiekens P, Mertens J, Verbruggen GJ. Silkworm and spider silk scaffolds for chondrocyte support. Mater Sci-Mater Med. 2008; 19:3399.
6. Kim HJ, Kim U, Kim HS, Li C, Wada M, Leisk GG, Kaplan DL. Bone tissue engineering with premineralized silk scaffolds. Bone. 2008; 42:1226. [PubMed: 18387349]
7. Peh RF, Suthikum V, Goh CH, Toh SL. Novel electrospun-knitted silk scaffolds for ligament tissue engineering. World Congress on Medical Physics and Biomedical Engineering. 2006; 14:3287.
8. Nair LS, Bhattacharyya S, Laurencin CT. Development of novel tissue engineering scaffolds via electrospinning. Expert Opin Biol Th. 2004; 4:659.
9. Damrongrungruang T, Siritapetawee M, Kamanarong K, Limmonthon S, Rattanathongkom A, Maensiri S, Nuchadomrong S. Fabrication of electrospun Thai silk fibroin nanofibre and its effect on human gingival fibroblast: A preliminary study. J Oral Tissue Engin. 2007; 5:1.
10. Zuo B, Dai L, Wu Z. Analysis of structure and properties of biodegradable regenerated silk fibroin fibers. J Mater Sci. 2006; 41:3357.
11. Xu Y, Shao H, Zhang Y, Hu X. Studies on spinning and rheological behaviors of regenerated silk fibroin/N-methylmorpholine-N-oxide.H_2O. J Mater Sci. 2005; 40:5355.
12. Kim K-H, Jeong L, Park H-N, Shin S-Y, Park W-H, Lee S-C, Kim T-I, Park Y-J, Seol Y-J, Lee Y-M, Ku Y, Rhyu I-C, Han S-B, Chung C–P. Biological efficacy of silk fibroin nanofibre membranes for guided bone regeneration. J Biotechnol. 2005; 120:327. [PubMed: 16150508]
13. Kim UJ, Park J, Li CM, Jin HJ, Valluzzi R, Kaplan DL. Structure and properties of silk hydrogels. Biomacromolecules. 2004; 5:786. [PubMed: 15132662]
14. Chen X, Shao ZZ, Knight DP, Vollrath F. Conformation transition kinetics of Bombyx mori silk protein. Proteins. 2007; 68:223. [PubMed: 17436322]

15. Gosline J, Guerette P, Ortlepp C, Savage K. The mechanical design of spider silks: From fibroin sequence to mechanical function. J Exp Biol. 1999; 202:3295. [PubMed: 10562512]
16. Bogush V, Sokolova O, Davydova L, Klinov D, Sidoruk K, Esipova N, et al. J Neuroimmune Pharm. 2009; 4:17.
17. Hakimi O, Knight DP, Vollrath F, Vadgama P. Spider and mulberry silkworm silks as compatible biomaterials. Compos Part B-Eng. 2007; 38:324.
18. Agnarsson I, Kuntner M, Blackledge TA. Bioprospecting Finds the Toughest Biological Material: Extraordinary Silk from a Giant Riverine Orb Spider. PLoS One. 2010; 5:1.
19. Binyamin G, Shafi BM, Mery CM. Biomaterials: a primer for surgeons. Semin Pediatr Surg. 2006; 15:276. [PubMed: 17055958]
20. Sumper M, Kröger N. Silica formation in diatoms: the function of long-chain polyamines and silaffins. J Mater Chem. 2004; 14:2059.
21. Kröger N, Deutzmann R, Sumper M. Silica-precipitating peptides from diatoms - The chemical structure of silaffin-1A from Cylindrotheca fusiformis. J Biol Chem. 2001; 276:26066. [PubMed: 11349130]
22. Knecht MR, Wright DW. Functional analysis of the biomimetic silica precipitating activity of the R5 peptide from Cylindrotheca fusiformis. Chem Comm. 2003; 24:3038. [PubMed: 14703846]
23. Naik RR, Brott LL, Clarson SJ, Stone MO. Silica-precipitating peptides isolated from a combinatorial phage display peptide library. J Nanosci Nanotechno. 2002; 2:95.
24. Gimeno-Fabra M, Peroglio M, Eglin D, Alini M, Perry CC. Combined release of platelet-rich plasma and 3D-mesenchymal stem cell encapsulation in alginate hydrogels modified by the presence of silica. J Mater Chem. 2011; 21:4086.
25. Foo CWP, Patwardhan SV, Belton DJ, Kitchel B, Anastasiades D, Huang J, Naik RR, Perry CC, Kaplan DL. Novel nanocomposites from spider silk-silica fusion (chimeric) proteins. PNAS. 2006; 103:9428. [PubMed: 16769898]
26. Mieszawska AJ, Fourligas N, Georgakoudi I, Ouhib NM, Belton DJ, Perry CC, Kaplan DL. Osteoinductive silk-silica composite biomaterials for bone regeneration. Biomaterials. 2010; 34:8902. [PubMed: 20817293]
27. Huang J, Valluzzi R, Bini E, Vernaglia B, Kaplan DL. Cloning, expression, and assembly of sericin-like protein. The Journal of Biological Chemistry. 2003; 278:46117. [PubMed: 12963711]
28. Rockwood DN, Preda RC, Yücel T, Wang X, Lovett ML, Kaplan DL. Materials fabrication from Bombyx mori silk fibroin. Nat Protoc. 2011; 6:1612. [PubMed: 21959241]
29. Goormaghtigh E, Cabiaux V, Ruysschaert JM. Secondary structure and dosage of soluble and membrane-proteins by attenuated total reflection fourier-transform infrared-spectroscopy on hydrated films. Eur J Biochem. 1990; 193:409. [PubMed: 2226461]
30. Byler D, Susi MH. Examination of the secondary structure of proteins by deconvolved FTIR spectra. Biopolymers. 1986; 25:469. [PubMed: 3697478]
31. Susi H, Byler DM. Resolution-enhanced fourier-transform infrared-spectroscopy of enzymes. Methods Enzymol. 1986; 130:290. [PubMed: 3773736]
32. Kong J, Yu S. Fourier transform infrared spectroscopic analysis of protein secondary structures. Acta Bioc Bioph Sin. 2007; 39:549.
33. Barth A. The infrared absorption of amino acid side chains. Prog Biophys Mol Bio. 2000; 74:141. [PubMed: 11226511]
34. Kauppinen JK, Moffatt DJ, Mantsch HH, Cameron DG. Fourier self-deconvolution- a method for resolving intrinsically overlapped bands. Appl Spectrosc. 1981; 35:271.
35. Inoue S, Tanaka K, Arisaka F, Kimura S, Ohtomo K, Mizuno S. Silk fibroin of Bombyx mori is secreted, assembling a high molecular mass elementary unit consisting of H-chain, L-chain, and P25, with a 6 : 6 : 1 molar ratio. J Biol Chem. 2000; 275:40517. [PubMed: 10986287]
36. Iler, RK. The Chemistry of Silica. John Wiley & Sons; New York: 1979.
37. Tobler DJ, Shaw S, Benning LG. Quantification of initial steps of nucleation and growth of silica nanoparticles: An in-situ SAXS and DLS study. Geochim Cosmochim Ac. 2009; 73:5377.

38. Derjaguin BV, Landau L. Theory of the stability of strongly charged lyophobic sols and of the adhesion of strongly charged particles in solutions of electrolytes. Acta Physicochimica (URSS). 1941; 14:633.

39. Verwey, EJ.; Overbeek, JTG. Theory of the Stability of Lyophobic Colloids. Elsevier; Amsterdam: 1948.

40. Schroeder WA, Kay LM, Lewis B, Munger N. The amino acid composition of Bombyx mori silk fibroin and of tussah silk fibroin. J Am Chem Soc. 1955; 77:3908.

41. Robson, RM. Hand book of fibre Science and Technology. Lewin, M.; Pearce, EM., editors. Vol. IV. Mercel. Dekker Inc; New York: 1985.

42. Neurath, H. Chemistry, biological activity, and methods. New York: Academic press; 1953. The proteins.

43. Ha S-W, Gracz HS, Tonelli AE, Hudson SM. Structural study of irregular amino acid sequences in the heavy chain of Bombyx mori silk fibroin. Biomacromolecules. 2005; 8:2563. [PubMed: 16153093]

44. Yamaguchi K, Kikuchi Y, Takagi T, Kikuchi A, Oyama F, Shimura K, Mizuno S. Primary structure of the silk fibroin light chain determined by cDNA sequencing and peptide analysis. J Mol Biol. 1989; 210:127. [PubMed: 2585514]

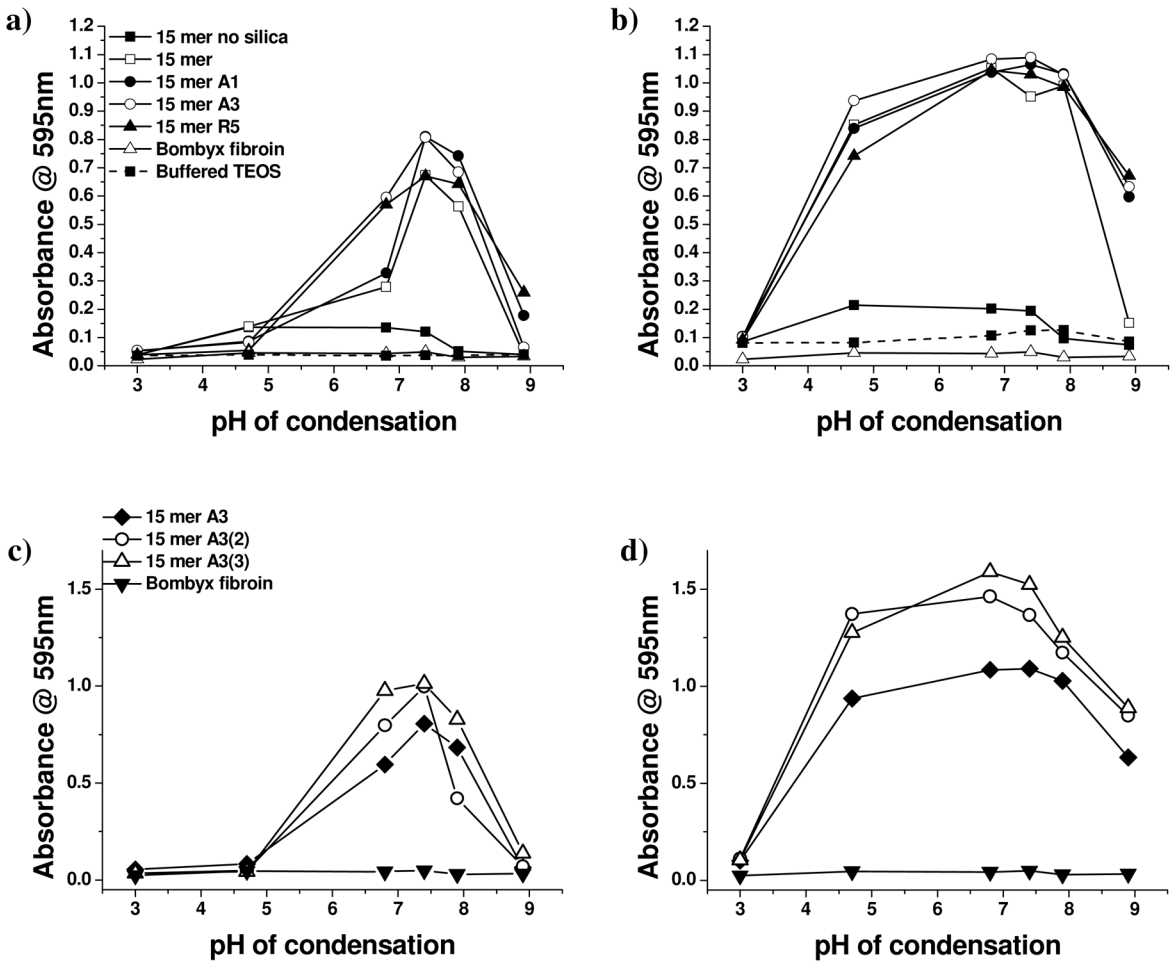

Figure 1.

Scattering intensity for samples with/without silk, silk chimeras and condensing silica after different periods of reaction, measured as absorbance @ 595nm. (a) 5 minutes condensation: 15mers and regenerated *B. Mori*, (b) equilibrium: 15mers and regenerated *B. mori*, (c) 5 minutes condensation: 15mer A3 chimeras, (d) equilibrium: 15mer A3 chimeras (legends for equilibrium data are the same as for 5 minute data).

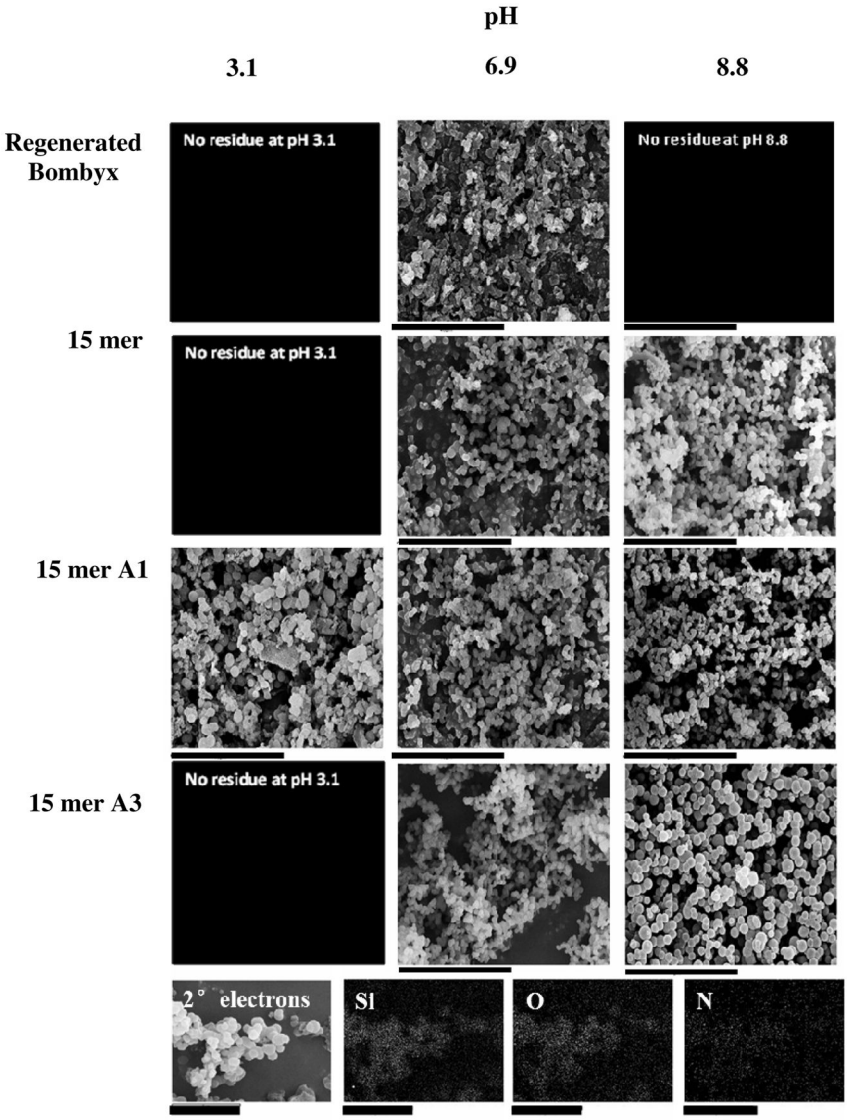

Figure 2.

Scanning electron microscopy images of siliceous structures deposited in the presence of Bombyx and recombinant silks. scale bars 40μm. Bottom row Example energy dispersive x-ray (EDX) analysis. 15mer A3 pH 6.9 Scale bars 5μm

3a).

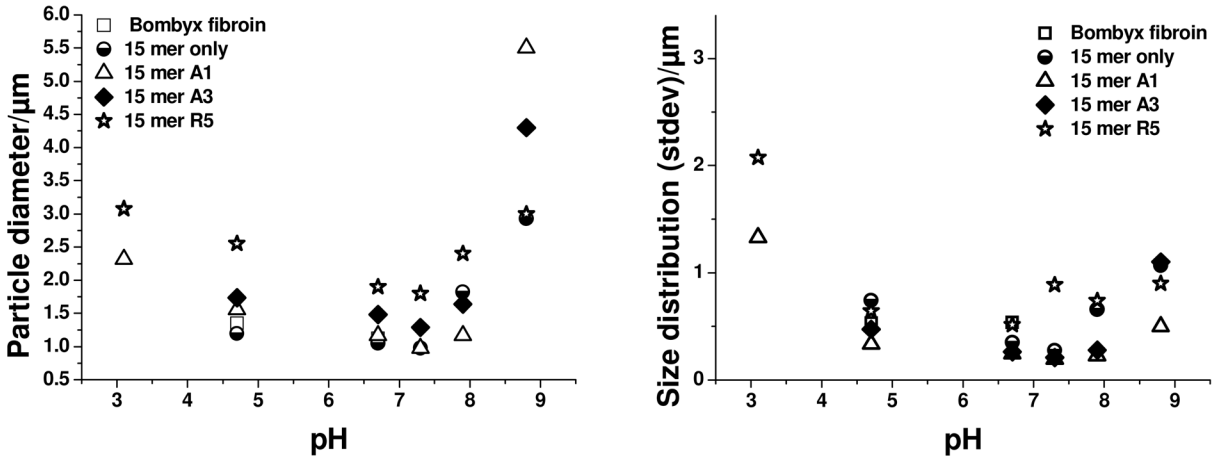

3b).

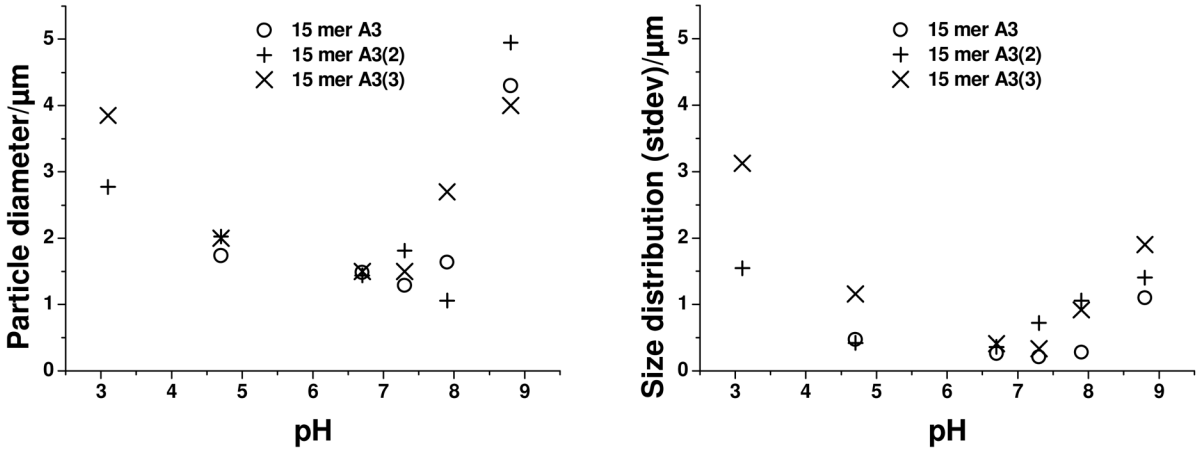

Figure 3.

Average particle size and dispersion of siliceous material isolated after condensation equilibrium time. a) 15 mer chimeras b) 15 mer A3 extended chimeras

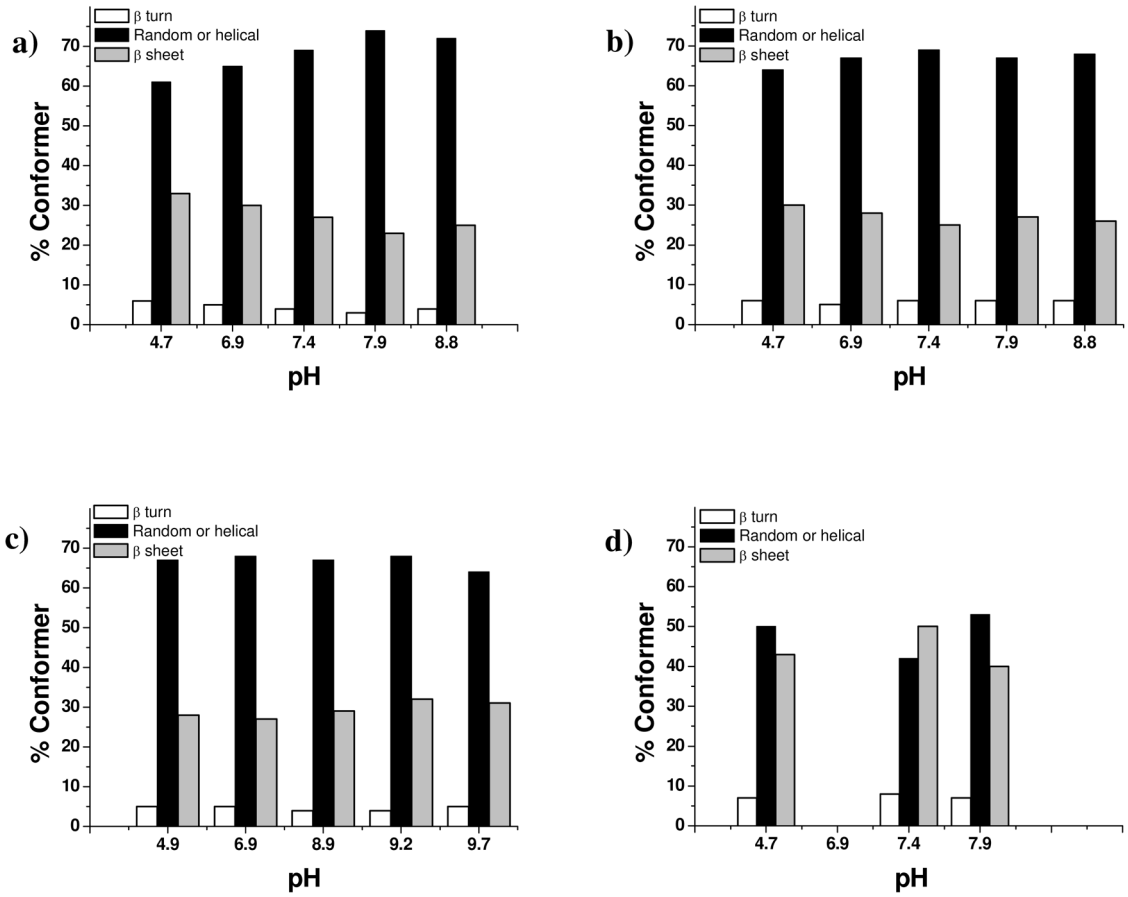

Figure 4.

Conformational change of silicified 15mers and regenerated *B. mori* fibroin with pH. a) 15-mer alone b) 15 mer A3 c) 15 mer A3(3) d) regenerated *B. mori* (insufficient residue for *B. mori* at pH 6.9 and 8.8).

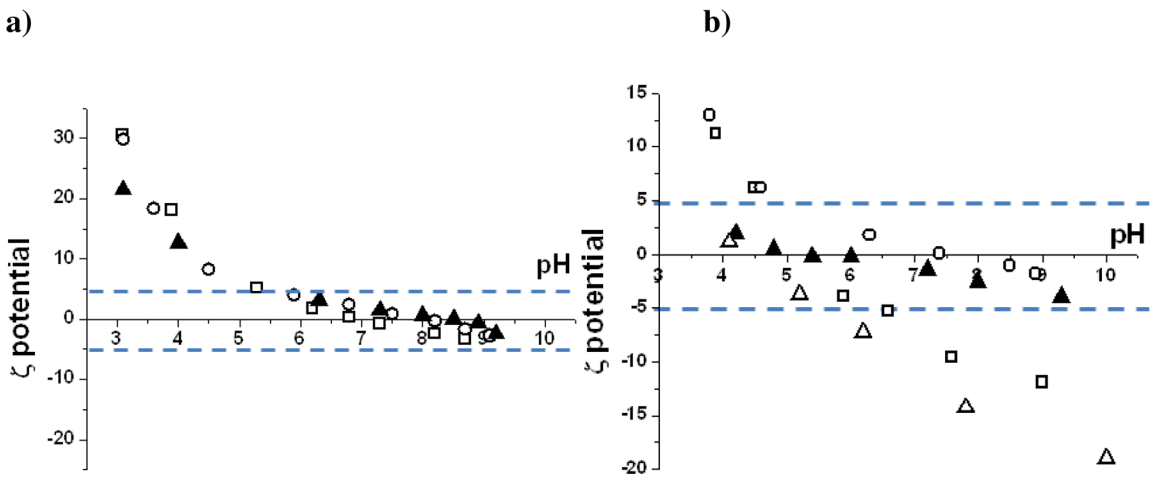

Figure 5.

Relationship between pH and surface charge of natural and chimeric silks. Zeta potential measurements for (a) □–15 mer A3, ○–15mer A3(2), ▲15mer A3(3) (b) △ regenerated bombyx, □ 15 mer non chimera, ▲15 mer R5 ○ 15 mer A1

The area between the lines represents the zone of highest colloidal instability

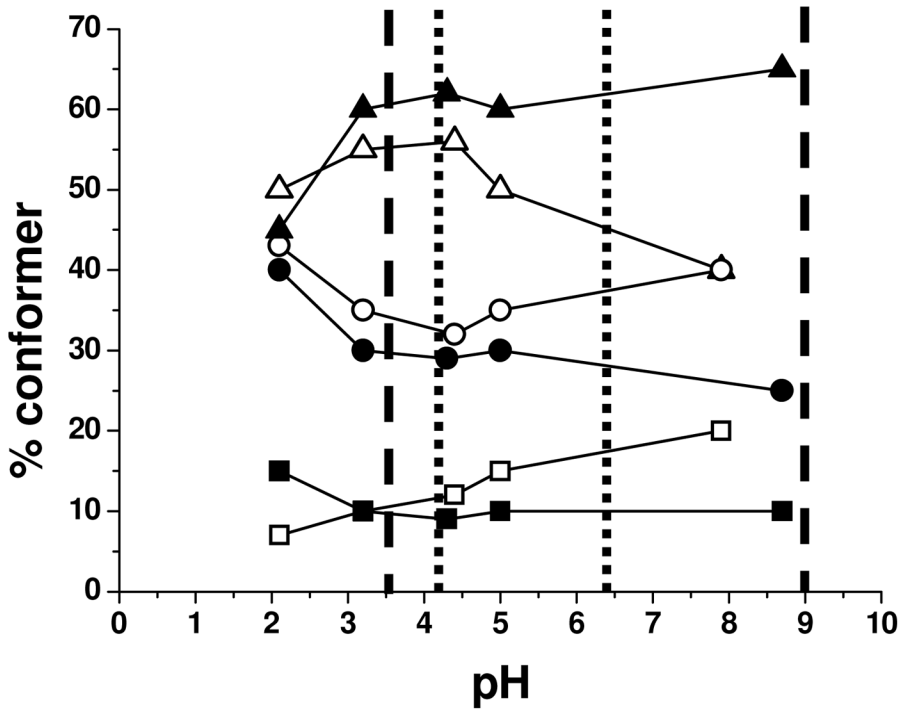

Figure 6.

Solution conformational analysis of recombinant proteins. 15 mers non chimera open symbols 15 mer R5 filled symbols. β turn ■, β sheet ●, α helix or random coil ▲. Lower and upper pH limit of maximum colloidal instability for 15 mer non chimera ----- and 15 mer R5 chimera — — —

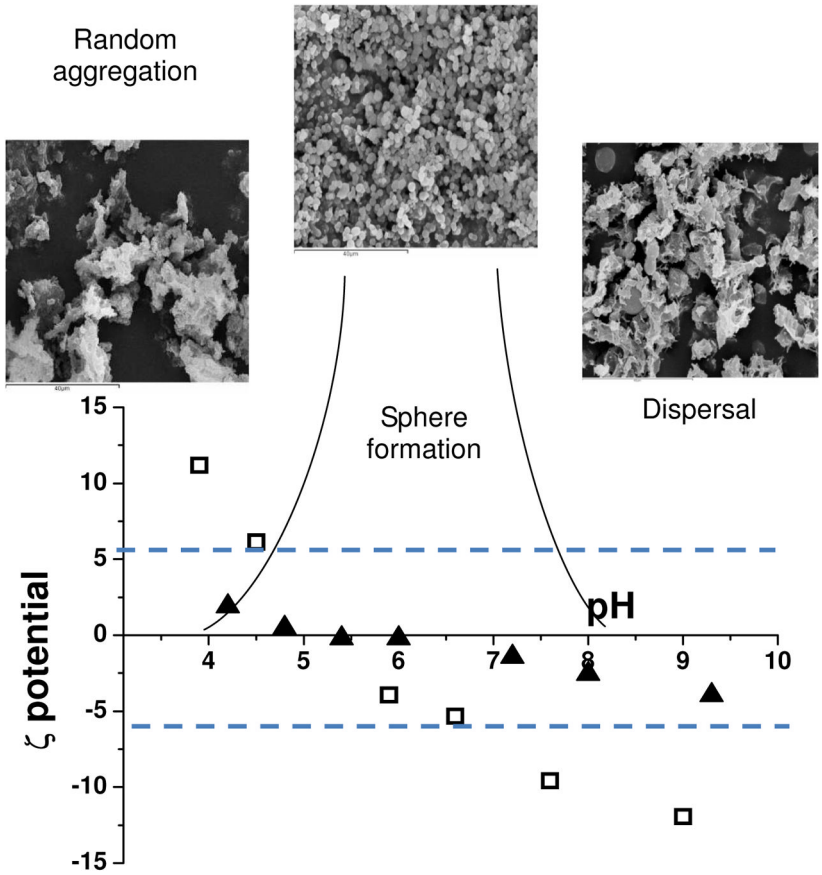

Figure 7.
Scheme showing control of silica sphere formation correlated with pH and zeta potential data for 15 mer-non chimera (empty squares) and 15mer-R5 (solid triangles) showing the zone of colloidal stability. SEM images scale bars 40μm

Table 1

Nominal formal charges on silks and chimeras used.

Silk/chimera identity (total amino acids)	Charged amino acids (identity and numbers present)
Silk (5471)[35]	77 (D,E) + 52 (R, H, K)
15-mer (487)	15 (R) + 6 (H in tag)
15-mer-A1 (498)	15 (R) + 6 (H in tag) + 2(K) + 2 (R)
15-mer-A3 (499)	15 (R) + 6 (H in tag) + 1(R) + 5(H)
15-mer-$(A3)_2$ (522)	15 (R) + 6 (H in tag) + $(1(R) + 5(H))_2$
15-mer-$(A3)_3$ (534)	15 (R) + 6 (H in tag) + $(1(R) + 5(H))_3$
15-mer-R5 (506)	15 (R) + 6 (H in tag) + 4(K) + 2 (R)